Ultrasensitive and miniaturized ion sensors using ionically imprinted nanostructured films

Antonio Ruiz-Gonzalez[a], Jingle Huang[a], Cao Xun[b], Roohi Chhabra[c], Roxanna Lee[d], Huang Yizhong[b], Andrew Davenport[c], Bing Li[a], Robert Palgrave[d], and Kwang Leong Choy[a,]*

a. Institute for Materials Discovery, University College London, London, WC1E 7JE United Kingdom.
b. School of Materials Science and Engineering, Nanyang Technological University, 50 Nanyang Ave, Singapore 639798
c. UCL Department of Renal Medicine, Royal Free Hospital, University College London.
d. Department of Chemistry, University College London, 20 Gordon Street, London, WC1H 0AJ, UK

Keywords: Ion imprinting, nanoporous silica, ion sensor

Abstract

The detection of ions is essential for a wide range of applications including biomedical diagnosis, and environmental monitoring among others. However, current ion sensors are based on thick sensing films (~100 μm), requiring time-consuming preparations, and they have a limit to their sensitivity of 59 mV.Log[C]$^{-1}$. Consequently, these sensors cannot be applied for high-precision applications that require high sensitivity and reduced dimensions. Furthermore, the research of anion sensors is hampered given the limited availability of molecular receptors or ionophores with acceptable performances. In this work, we overcome these limitations using a 300 nm thick sensing film based on nanoporous ion-imprinted core-shell silica/gold grafted onto a 50 nm gold film. The sensing films were highly selective towards chloride ions, compared to other anions such as nitrate, sulphate and carbonate. Moreover, this nanostructured film exhibited over 3-fold higher sensitivity (-186.4 mV.Log[C]$^{-1}$) towards chloride ions compared to commercial devices. This breakthrough has led to the fabrication of the smallest and most sensitive reported anion sensor working on open circuit potentiometry, with an exceptional selectivity towards chloride ions that could be used for the measurement of chloride ions in human serum.

Introduction

The quantification and monitoring of ions in solution is essential for a wide range of applications such as the clinical analysis, physiological monitoring[1-3], water quality evaluation[4] performance monitoring of energy storage devices[5], corrosion monitoring in structural engineering[6], or agricultural smart farming[7] among others. Specifically, anion imbalances play a key role in the development of multiple diseases such as chronic kidney disease[8] and can lead pathological conditions such as acidosis. Acidosis is caused by an accumulation of acid that can be a consequence of an excess of chloride ions, with deleterious effects in the body[9]. In addition, excessive presence of anions such chloride in aquatic environments can lead to the acidification of the environment or decrease the anti-microbial capability of treated water. Therefore, chloride concentrations must be tightly regulated[10]. From an industrial perspective, the presence of chloride ions is a strong indicator of environmental degradation processes such as corrosion[6] and the quality and health of the structural engineering materials[11]. However, due to the generally small size of anions, less than 0.2 nm in the case of chloride ion (Cl^-), and their scarce lipophilicity[12], only a few commercial anion sensors are currently available in the market, and the number of reported approaches in the literature is limited. Most of these sensors also exhibit a rather poor performance due to ionic interferences and hence low selectivity[13].

Although there is a demand for miniaturized anion sensing devices with super-sensitivity, greater than the Nernst limit of 59 mV.Log$[C]^{-1}$ for the measurement of anions for high-precision applications, to date, no approaches have been able to fulfil such requirements. Traditionally, the main technology for the development of ion-selective electrodes consists of a plasticized PVC membrane with embedded ionophores, which are specific complexing agents that perform the electrolyte recognition process[14]. However, numerous studies have been focused on the formalization of ion-selective electrodes theory[15-18], and concluded that the sensitivity of the devices is thermodynamically limited to 59 mV.Log$[C]^{-1}$[14]. In addition, their miniaturization has been proven to be challenging, and typical sensors tend to be thick, with a typical thickness in the range of 100 μm[19].

Early attempts in the miniaturization of ion-selective membranes membranes showed a faster ion equilibration kinetics when they were reduced to 35 μm thick layers[20]. However, no sub-

micron level films operating at zero-current conditions have been reported in the literature. Such level of reduction could offer advantages in terms of the time-response of the sensors and allow a better integration in miniaturized systems, especially desirable for portable or wearable technologies. As such, an enhancement in the sensitivity and miniaturization of the ion sensors would be beneficial for portable and wearable applications. The miniaturization of the sensing materials would also be beneficial to interface this sensor technology with upcoming technologies such as ion-selective field effect transistors[21]. In addition, the development of rapid sensors operating with super-sensitivity beyond the Nernst limit is crucial to characterize the concentration of ions locally around neurons, which could help in the diagnosis of seizures[22], and even allow genome sequencing[23].

As mentioned, the performance of commercial and state-of-the-art ion sensors based on ionophore-containing polymeric films are constrained to the use of relatively thick sensing films, in the range of micrometers, and a restricted sensitivity of 59 mV.Log[C]$^{-1}$. Shklovskii *et al.*[24, 25] observed that this sensitivity limit could be surpassed when charged surfaces are employed, offering the possibility of developing a new family of sensors with super-Nernstian sensitivities. This observation was a consequence of the strong interaction between the opposite charges of ions and the membranes. Although this work was based on the study of macroions, recently Sivakumarasamy *et al.*[26] demonstrated the suitability of this concept to develop an ion-sensor based on specific sites on a 25 nm 0D transistor using a silica surface for the simultaneous detection of multiple cations in serum. However, the costly fabrication methods, based on nanolithography and their sensing mechanism, requiring complex nanofluidic channels, led to challenging data analysis, due to the necessity of modelling the response of the sensor in the presence of multiple electrolytes. This has not only been translated into a large uncertainty on the measurements and sensing data but also it has led to an impracticable technology commercially. Moreover, this device configuration could not be used for the determination of negatively charged ions such as chloride ions. Since then, multiple ionic exchange resins have been developed for the adsorption of multiple ions, limited to cations such as zinc[27], nickel[28] and lead[29, 30]. However, these materials lacked specificity, limiting their suitability as components of ion sensors, and in general there is a lack of advances in the field of anion-selective materials. Recently, Chen *et al.*[31] reported a silica/methacrylate hybrid material for the removal of specific toxins from patient's blood. This material consisted of a hierarchically porous particles, containing a silica nanoparticle-based core, and a polymerized methacrylate hydrogel shell. The molecularly imprinted

hydrogel hybrid material could remove known toxins (i.e.urea, lysozyme, creatinine) with high efficiency and selectivity using a microfluidic chip, with absorption efficiencies over 75%. However, the electrochemical detection of toxins concentrations using this method was not explored. In addition, the discovery of materials for the selective detection of anions represents a major challenge in analytical chemistry, electrolyte monitoring in patients, diagnosis, and anion measurement for environmental evaluation.

The exploitation of imprinted technology for the fabrication of sensing materials represents a promising alternative in this field, allowing the development of tailor-made sensing electrodes with reduced dimensions. The material imprinting process is based on the synthesis of sensitive species by direct polymerization of functional monomers in the presence of a template. Thus, specific recognition elements can be developed virtually for any compound[32, 33]. To date, this approach has been applied mostly to the detection of cations, including copper[34-36], cadmium[37, 38], mercury[39] and lead[40], and rare earth metal ions such as europium[40] and yttrium[41]. Specifically, the use of silica nanoparticles as molecularly imprinted materials for sensing represents a promising approach in the field, given the versatility of the synthesis, allowing multiple shapes and porosities, and the possibility of modification with multiple surface chemical groups. Silica nanoparticles have previously been combined with conductive materials such as star-shaped gold nanoparticles[42], for the detection of antibiotics using Surface-Enhanced Raman Scattering. The use of these star-shaped nanoparticles increased the sensitivity of the Raman Scattering process, leading to a limit od detection within the nanomolar level. As such, the morphology of silica nanoparticles can be tailored for multiple compounds. The pore size and composition of silica nanoparticles can additionally be modified, allowing a detection of different compounds. Xie *et al.*[43] reported a silica-based nanomaterial that could be used for the detection of TNT. This material combined the positive charged of quaternary amines, and a specific pore shape for the specific detection of this compound, leading to highly monodispersed silica nanoparticles. However, due to the weak interaction of the anions with the chelating species commonly reported in the literature, thus far there has been a limited development in this field. Although similar imprinting approaches have been applied to the fabrication of sensing materials for the detection of relatively small anions such as phosphate and nitrate ions[44, 45] for potential applications in environmental monitoring, its potential for the specific interaction with single anions such as chloride ions has yet to be explored.

Within the present work, a miniaturized device with 300 nm thick nanostructured sensing film was developed by exploiting the ion imprinting technology with a novel material functionalization and grafting methods. The new device structure reported here is based on the use of a porous core-shell configuration with gold nanoaggregates and a shell of nanoporous silica containing positively charged amine groups. These positively charged amine groups enhanced the sensitivity of the sensors and greatly reduced the preparation and pre-conditioning time. The Au nanoparticles were synthesized to be specific towards chloride by condensing silica monomers in the presence of HCl, and using gold nanoaggregates as the core material. Such a material transformed the typical signal transduction mechanism of the traditional sensors based on the bulk diffusion of electrolytes, into a surface effect through the adsorption of ions. Such novel materials and sensing device configuration reported here enabled the development of the smallest Ion sensor working on Open Circuit Potential (OCP) with an unprecedented sensitivity and selectivity.

Results and discussion

Structure of the nanostructured sensing layer

The first step in the development of the nanostructured sensors was the characterization of the fabricated gold nanoclusters. Gold nanoclusters were synthesized by a simple reduction method using citric acid. In this case, gold was used for the transduction of the electrochemical signal due to its strong interaction with chloride ions[46] and its low charge transfer resistance[47]. A solid shell of nanoporous silica using tetraethyl orthosilicate (TEOS) as a precursor was then integrated, increasing the specificity of the sensor, and allowing the attachment to the gold contact. In addition, the amine group present in aminopropyl triethoxysilane (APTES) were used as the recognition element towards chloride ion species. This functional group was proven to be versatile, enhancing the interaction with the anions after being positively charged using an acidic solution of HCl.

The specificity of this material was accomplished by the synthesis of the TEOS and gold precursors in the presence of HCl, which contains the target ion Cl^-, allowing the formation of a specific pore structure in this material. The structure of this recognition element, using a porous silica as the receptor located on the outer shell of the sensor, was confirmed by high resolution transmission electron microscopy (HRTEM) (Figure 1.a) and Figure 1.b)). Most of the gold particles used as the core were formed along the zone axis of [1 0 1], with [1 1 1] being the strongest crystallographic orientation (Figure 1.c)), and the distribution of both gold

and silica could be observed using the Z-contrast (Figure 1.d) and Figure 1.e)). Both elements could be observed together within the core-shell structure of the ionically imprinted gold/silica nanoparticles (Figure S.1). The synthesized gold nanoclusters were homogeneous in size, typically in the range of 5 nm, and they were crystalline as confirmed by the strong diffraction spots in the Fast Fourier Transform (FF) pattern.

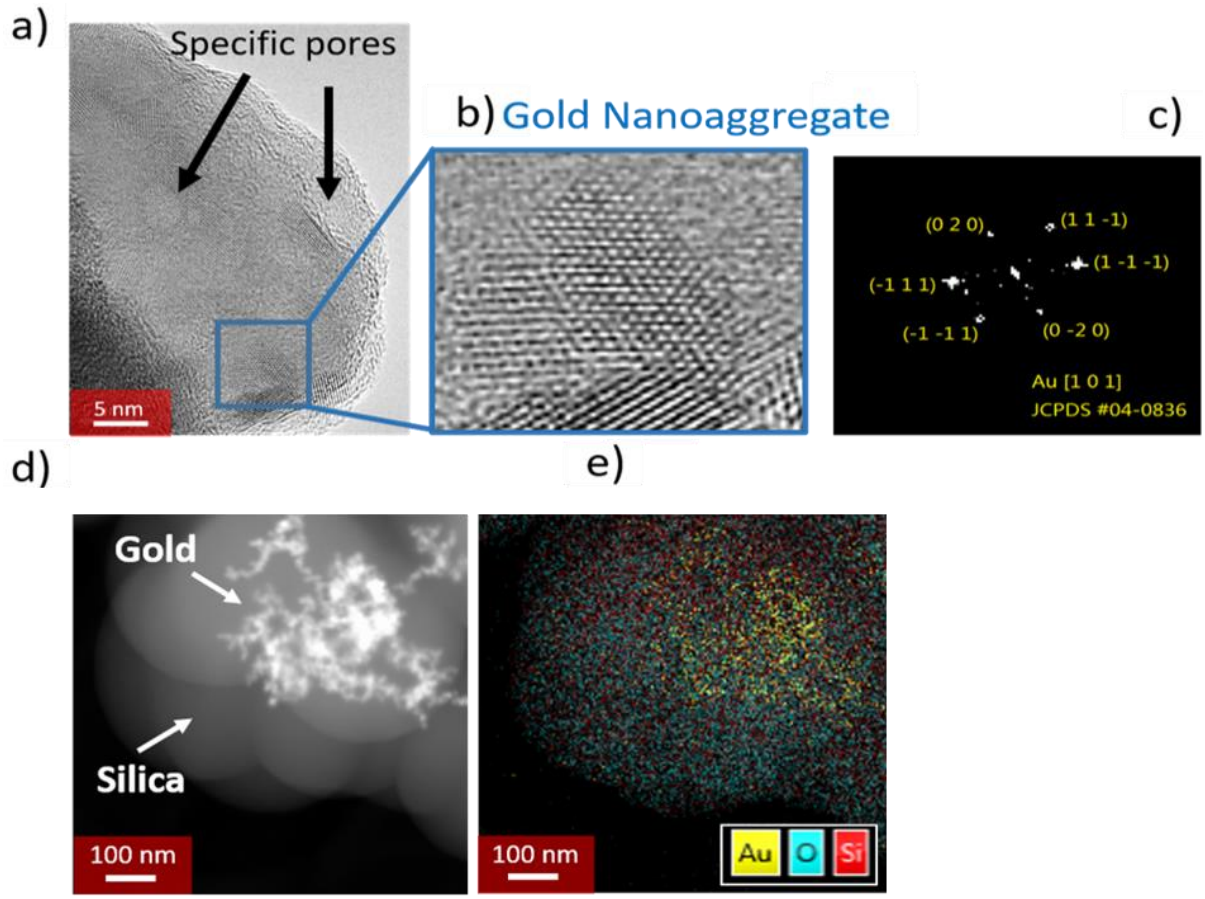

Figure 1. HRTEM visualization of the silica-Au core-shell structure. **a)** Detail of the surface of the ionically imprinted silica onto the gold nanoclusters where the pore structure is highlighted with pore diameter typically around 3 nm. **b)** A gold nanoaggregate is magnified, allowing the visualization of the crystalline structure. **c)** FFT diffraction pattern showing the presence of gold with [1 1 1] as the preferred orientation. **d)** HAADF-STEM revealing the distribution of both silicon and gold elements across the core-shell structure using a Z contrast. **e)** EDX mapping of Au (yellow) and Si (Pink) indicating the distribution of both elements within the ionically imprinted Gold/silica nanoparticles.

A porous structure was formed within the ionic imprinted silica/gold, which was consistent with the previous work in silica-based nanoimprinted particles[48]. The pore radius here observed was confirmed by BET, being in the range of 1.4 nm (Figure 2.a)), and a total surface area of 108 m^2 g^{-1}. This surface area was calculated from the isotherms obtained using BET and the associated BET equation (Figure S.2). The pore size is comparable to previous ion imprinted systems based on silica nanoparticles for dissolved metals[49, 50]. The determined pore size was compared to the one obtained in the case of non-imprinted nanoparticles, synthesised by employing a similar method as in the case of Gold/silica nanoparticles, but without the incorporation of HCl within the precursor solution.

The isotherms for the non-imprinted Gold/silica nanoparticles are shown in Figure S.3.a.The pore size of the non-imprinted nanoparticles was in the range of 0.8 nm, smaller than the one obtained in the case of non-imprinted nanoparticles (Figure S.3.b.). However, in this case, the estimated cumulative pore volume was 31.1 mm^3 nm^{-1} g^{-1}, which was lower than the one obtained in the case of the silica/gold ionically imprinted nanoparticles, in the range of 55.7 mm^3 nm^{-1} g^{-1}. These results indicate a higher concentration of pores within the surface of the ionically imprinted nanoparticles, which was proven to be crucial for the sensing performance of the devices.

The spherical architecture of the ionically imprinted nanoparticles, with a size in the range of 118±29 nm after the synthesis, was further corroborated by SEM (Figure 2.b) and Figure S.4). The nanoparticle grafting on the gold electrodes was carried out by a directional attachment of APTES via EDC/NHS chemistry. A successful anchoring of molecularly imprinted polymeric nanoparticles has been achieved in the literature by previous functionalization with primary amines and posterior reaction with the substrates[51]. However, this process had to be modified in our nanoimprinted material since the direct use of the EDC reagent could modify the amine groups present in the specific recognition sites, leading to a loss in sensitivity. Here, the gold electrodes were first functionalized using a self-assembled monolayer of 16-mercaptohexadecanoic acid. A directional attachment of APTES using the standard 1-Ethyl-3-(3-dimethylaminopropyl)carbodiimide and N-Hydroxysuccinimide (EDC/NHS) chemistry was then employed, grafting the molecules and exposing the silane groups that could interact with the nanoparticles. Finally, the nanoparticles were deposited.

The chemical characterization of the nanoimprinted material was performed using FTIR (Figure 2.c)) which revealed the typical spectrum of APTES, with a peak in the 1390 cm^{-1} range, indicative of the -CN stretch. The 1032 and 778 cm^{-1} peaks were also detected due to the presence of the Si-O-Si structure of silica[52]. This 2-step approach for the fabrication of the sensing devices could be applied to the production of an array of up to 5 electrodes onto a glass substrate (Figure 2.d)).

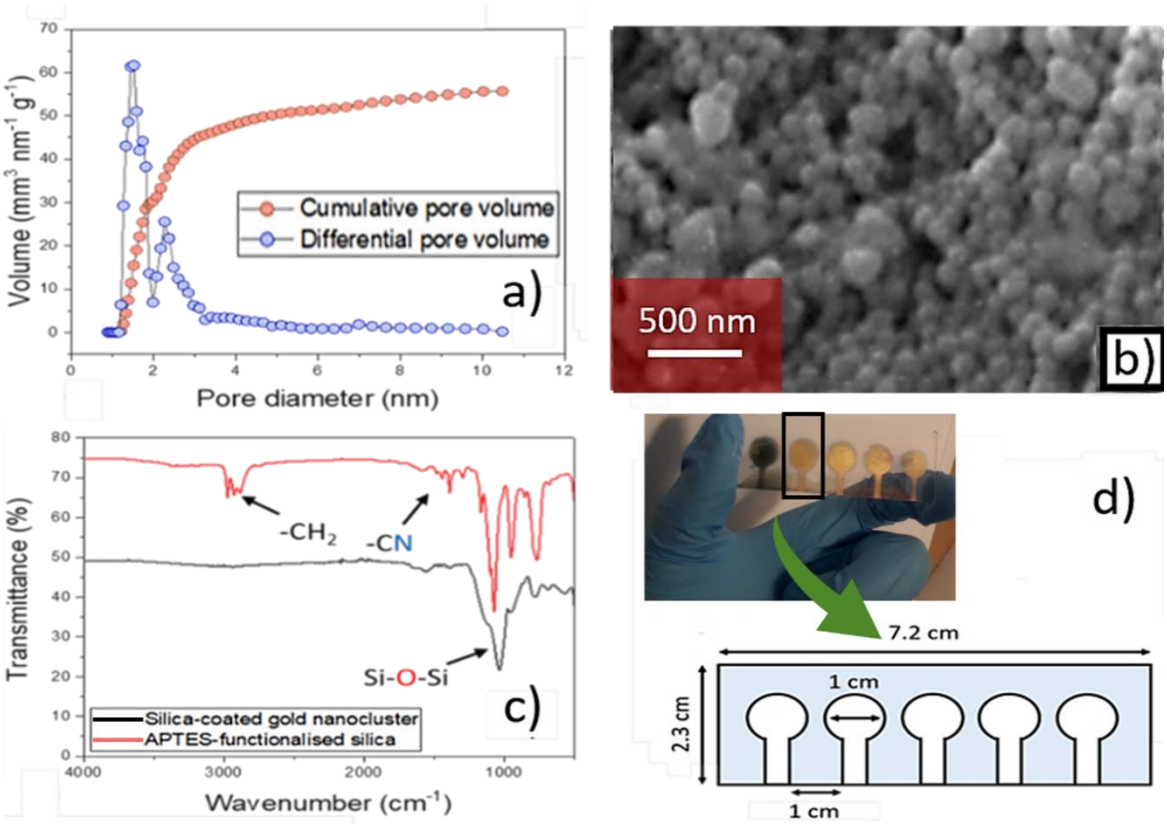

Figure 2. a) Cumulative and differential pore volume obtained by BET, showing a higher presence of pores in the 2.8 nm range. **b)** SEM image of the silica encapsulated gold nanoparticles. **c)** FTIR spectrum of the silica-encapsulated gold when compared with the one obtained for APTES-functionalized silica. The representative peaks of the Si-O-Si bonds present in silicon dioxide (1032 and 778 cm^{-1}) and APTES (-CH_2 at 3000 cm^{-1} and -CN in the range of 1600 cm^{-1}) are highlighted. **d)** Picture of the thin film sensing device containing the grafted ionically imprinted silica nanoparticles on the surface of gold electrodes. The dimensions of the sensors are highlighted.

Sensing mechanism

Since our nanostructured sensing film is based on nanoporous core/shell silica/gold nanoparticles, its sensing mechanism is a consequence of the adsorption of ions on the surface of the nanomaterials. This mechanism has been proven by multiple simulations studied on molecularly imprinted materials. In this case, the particular molecular structure of the silica shell, forming a specific pore with a specific disposition of functional groups and ligands, in combination with the stoichiometry employed, allowed the formation of a highly sensitive and selective sensing film. The ions present in solution in a solvated form, surrounded by a water shell (Figure 3.a)) can interact with the amine groups at the surface of the nanoporous core/shell silica/gold nanoparticles (Figure 3.b) and Figure 3.c)).

The detection mechanism of the gold/silica imprinted nanoparticles was confirmed by XPS. Initially, the presence of APTES amines was studied (Figure S.5). Two different samples were studied in this case; pristine molecularly imprinted gold/silica nanoparticles, that had been washed with DI water after synthesis, and molecularly imprinted gold/silica nanoparticles that had been exposed to 10 mM HCl before the study using XPS. The Si 2p scans for both samples confirmed APTES functionalization. The main Si environment in SiO_2 is a $Si(-O)_4$ binding environment around 103.6 eV, and there is a $Si(-O)_3$ binding environment component around 101.4 eV due to APTES binding to the surface[53]. Each environment is split into a doublet by spin-orbit coupling. The energy separation for the Si 2p doublet in SiO_x compounds is 0.6 eV[54].

The presence of quaternary amines within the surface of the gold/silica imprinted nanoparticles was additionally studied. As mentioned, the amines present in APTES can exist as a NH_3^+ group, a hydrogen-bonded NH_2 group (NH_2---H) or a free NH_2. Two peaks were observed using high-resolution XPS on the amine group region within both control, and HCl-exposed samples. The higher binding energy peak ~ 402.0 eV indicates the NH_3^+ / NH_2---H environment and the peak at ~ 399.9 eV arise from the free NH_2 group[55] (Figure 3.d. and Figure 3.e.). This peak was present in both pristine and HCl-treated samples. The higher intensity of 402.0 eV in the HCl treated sample is consistent with the electrostatic adsorption of Cl^-. The presence of chloride was additionally measured within the surface of the HCl treated nanoparticles. These results are indicative of the adsorption mechanism of these nanoparticles based on electrostatic adsorption of Cl^- onto the positively charged NH_4^+ amines. The Cl 2p peak is split into a doublet by spin-orbit coupling (Figure 3.f.).

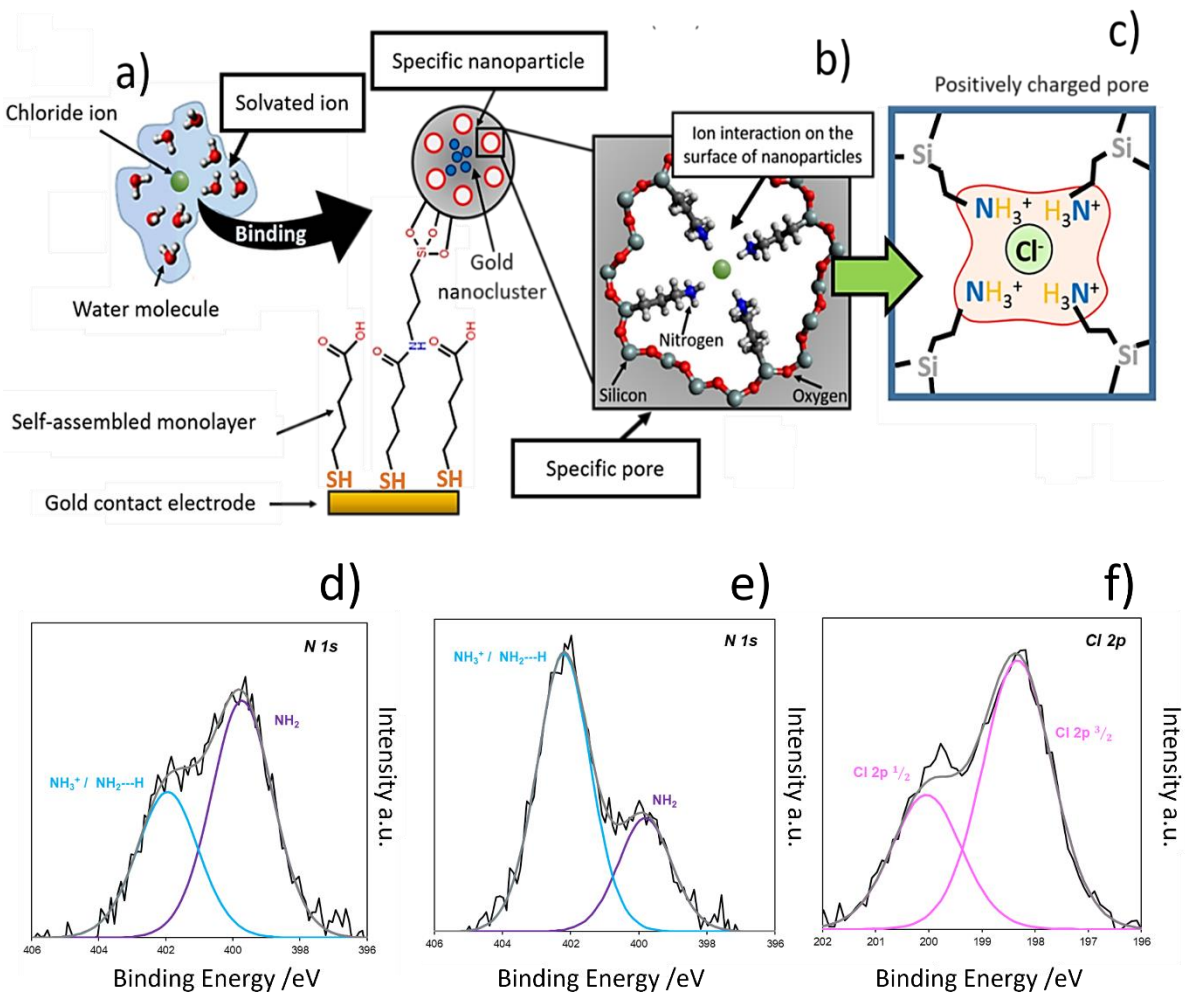

Figure 3. a) Proposed principle of ion recognition process by imprinted nanoparticles. The solvated chloride ion (green) is present in solution with a water shell, and a binding site on the silica surface (red). with a size specific achieved via HCl templating process to chloride ions and amine groups for the complexation is distributed around the silica-gold nanoparticulate film surface. **b)** The ion is complexed in the binding site containing the amine groups (blue), allowing the measurement of its concentration by measuring the changes in the potential. **c)** Molecular representation of the possible interaction process taking place in the pore cavity of the silica shell between the positively charged amine groups and the chloride ions. The red area indicates the presence of a positively charged environment. **d)** Binding energy from amine groups measured in pristine molecularly imprinted silica/gold nanoparticles, washed twice using DI water after the synthesis. **e)** Binding energy measured on gold/silica molecularly imprinted nanoparticles after exposure to 10 mM HCl. **f)** Binding energy measured from Cl detected in HCl-treated gold/silica molecularly imprinted nanoparticles.

Ion imprinted silica/gold nanoparticles on the sensing layer can address the thickness and sensitivity limitations of conventional membrane-based ion-selective electrodes by offering specific binding sites directly exposed to the sample. Consequently, the sensitivity of the electrodes will be triggered by surface effects, due to the adsorption of chloride ions onto the sensitive silica-gold nanoparticles, instead of the traditional bulk diffusion. This new mechanism allows the sensitivity to go beyond the traditional Nernst limit and permit the size of the sensing electrodes can be reduced. Gold nanoclusters were employed due to their low charge transfer and electrical resistances and their affinity towards chloride ions[46, 56]. These gold nanoaggregates provided support for the formation of the selective silica shell during the synthesis of the films as depicted in Figure S.6. In addition, such gold nanoaggregates improved the conductivity of the nanoparticles, since the low conductivity of silica could hinder the electrochemical transduction of the sensors. Such effect of improved conductivity has been reported in the case of molecularly imprinted sensors[57]. In the present work, the use of gold was fundamental for improving the sensitivity rates of the ion sensors by improving the signal transduction. When no gold was employed during the sensitivity of the devices towards Cl^- ions was -66±7 mV.Log$[Cl^-]^{-1}$ when using NaCl salts for the calibration. This value was significantly lower than the value reported when gold was used as the core material for the ionically imprinted nanoparticles, which was in the range of -186 mV.Log$[Cl^-]^{-1}$, confirming the role of the gold nanoaggregates in the sensing. On the contrary, when higher concentrations of gold were used, no significant changes in the sensitivity of the final devices were observed. When 10 mL of the gold dispersion solution was employed instead of 5 mL during the synthesis process, a sensitivity of 176.8 mV Log$[Cl^-]^{-1}$ was obtained. In addition, the detection limit remained within the mM level (Figure S.7.). However, the linear range of the devices decreased, reaching a maximum linear limit around 80 mM, while the devices containing only 5 mL showed a linear response up to 100 mM. This result indicates that the incorporation of 5 mL was enough to provide a good conductivity to the Gold/silica nanoparticles. A volume of of 5 mL was also proven to be optimal in terms of sensing performance of the films.

During the synthesis, the affinity of the gold surfaces towards chloride ions allowed the selective adsorption of such chloride ions onto the surface of the gold nanoaggregates during the synthesis of the core/shell silica/gold nanoparticles. The presence of chloride ions onto the gold nanoaggregates facilitated the interaction of anions with the TEOS and APTES monomers during the condensation onto the gold nanoaggregates (Figure S.6). Thus, the

presence of gold nanoaggregates during the synthesis of the core/shell silica/gold nanoparticles was necessary for the formation of the selective silica shell.

The novel chloride ion sensing concept demonstrated here employed a chloride ion-specific electrode based on an amine-functionalized ion imprinted porous silica shell, with nano pore sizes (circa. 1.4 nm in radius). This structure allowed the miniaturization of the device while ensuring a proper signal transduction and enhanced the selectivity of the device. APTES was used as the recognition agent by quaternisation of the amines present on its molecular structure for the sensing Cl^- species through the use of HCl, generating a positively charged surface on the imprinted nanoporous silica shell. The use of these positively charged APTES monomers reinforced the electrostatic interactions between the silica/gold nanoparticles and the target chloride anion. The performance of this ion sensor remained stable at relatively low pH values (3-7). However, at higher pH values, in the range of 11, the sensitivity of the devices decreased, from -186±10 mV.Log$[Cl^-]^{-1}$ when a pH of 7 was used up to a standard Nernst sensitivity of -54±4 mV.Log$[Cl^-]^{-1}$ when the pH reached 11 (Figure S.8). This decrease in the sensitivity was a consequence of the de-quaternisation of the APTES, which takes place at basic pH values, but it is not expected to have a significant impact when working with biological solutions. This effect was reported by Hamza *et al.*[58], who described the higher absorption rate of uranium ions in the presence of quaternary amine groups. As such, the involvement of the quaternary amine groups from the APTES in the sensing was confirmed, which allowed the potentiometric detection of chloride ions in the electrolytes. The decrease in sensitivity due to pH changes could be tackled in the future by the use of buffer hydrogels. Agarose-based hydrogel microemulsions have been developed as pH buffer components without impacting on the selectivity of ion-exchange resins[59]. These materials could be employed as coatings for the gold/silica sensing nanoparticles described in this work. Although this approach could potentially increase the thickness of the films, it shows promise to enhance the sensing performance. In addition, alternative positively charged functional groups such as tetramethyl ammonium-based groups could be used with lower sensitivity towards pH changes. However, the availability of siloxane-based tetramethyl ammonium groups that can be easily incorporated within a porous silica matrix is limited.

Demonstration of the sensing performance of the ultra-thin Imprinted ion sensor

After grafting the nanoparticles onto 50 nm thick gold electrodes with an APTES linker, a 290 nm thick nanostructured film was obtained as measured by a stylus profilometer (Figure

S.9). To the best of our knowledge, this is the smallest reported potentiometric ion sensor based on OCP readings. The efficiency of this grafting process over time was estimated by imaging the electrodes surface at different times after exposure to the nanoparticle by using SEM (Figure S.10.). This experiment allowed us to determine the optimal deposition time for the fabrication of sensors. After 1 h of incubation, the coverage of the deposited nanoparticles covered only ~15% of the total area. However, this deposition area greatly increased after 4 h, reaching over 98%. As such, this time was selected as the minimum incubation time required for the deposition of the sensing electrodes.

After the fabrication of the full device, a homogeneous film was obtained, with the presence of regularly distributed domains rich in ion imprinted nanoparticles containing gold. This surface morphology of the film consisting of ion imprinted nanoparticles, formed small aggregates in the range of 500 nm as observed by SEM equipped with EDS elemental mapping (Figure 4.a)).

The attachment of the ion imprinted nanoparticles to the electrodes using the covalent bond with the APTES linker here reported was analyzed by quartz microbalance. This technique can be used for the determination of weight changes over an electrode in the nanogram range, confirming the success of the functionalization due to the changes in the mass on the electrodes in Figure S.11)). Within the first step of the fabrication, where the APTES group was directionally grafted after the deposition of the self-assembled film, a gain of 188±20 $ng.cm^{-1}$ was observed. The post-modification with silica/gold nanoparticles increased the total weight by 294±3 $ng.cm^{-1}$, being consistent with the two-step approach for the nanofilm fabrication. This technique could additionally be employed for the determination of the total amount of adsorbed chloride ions on the surface of the ion imprinted porous silica/gold nanoparticles. Such a test was used to confirm the relevance of using the chloride ion templates during the synthesis. In this case, the differences in the mass of the sensors during the conditioning in DI and after their immersion in 0.1 M KCl solution was recorded, and normalized by dividing the result by the initial weight of the films in DI water.
An absorption ratio of 8.1 $\Delta ng_{ion}.ng_{eq}^{-1}$ was obtained when templated gold/silica ionically imprinted nanoparticles were employed. On the contrary, when no HCl was employed, also called non-templated ion imprinting nanoparticles, a significantly lower absorption with a maximum of 3.4 $\Delta ng_{ion}.ng_{eq}^{-1}$ was obtained as shown in Figure 4.b). Consequently, these non-templated ion imprinting devices could not be employed for the sensing. This lower

absorption could be attributed to the reduced formation of nanopores and the low presence of charged functional groups.

A final test of the electrochemical performance was subsequently performed on the sensing device. The OCP of the ion sensor was used as the measurement method, similar to the case of the commercial polymeric based sensing films, which tends to require a low energy consumption. Contrary to the standard commercial polymer-based ion-selective sensors, the devices employed here did not require a long pre-conditioning process. The commercial sensors typically need to be subjected to a highly concentrated solution in the range of 0.1 M of the target analyte for at least 24 h to reach equilibrium before their usage[60]. Consequently, they require time-consuming preparation for such preconditioning process. However, the present ion sensing device could reach the equilibrium with the solution shortly after the synthesis, and only 46 mins were required to reach the equilibrium (Figure S.12.a. and Figure S.12.b.)). The signal drift of the ion sensors was in the range of 1.1 mV h^{-1} (Figure S.12.c.), being significantly lower than the standard commercialized devices for anions, in the range of 5 mV[61], and was stable for at least 13 h under constant contact with the solution. In addition, the electrochemical noise of the devices was in the range of 0.4 mV min^{-1} (Figure S.12.d.). Thus, the ion sensing devices could be applied to the continuous measurement of electrolytes due to the rapid nature of the adsorption reaction, offering a prompt monitoring of analytes.

When using metal salts that contained chloride ions such as NaCl, KCl or $CaCl_2$, a super-Nernstian response in the range of -186.4 mV.log$[Cl^-]^{-1}$ was achieved within the linear range of the plots, with a limit of detection in the range of 10^{-4} M (Figure 4.c)). This value overcomes the traditional Nernst sensitivity limit of -59 mV.Log$[C^-]^{-1}$, representing a new record in the performance of these anion sensors, specifically chloride ions. The sensitivity in this case was calculated by measuring the slope of the responses within the linear range of the measurements (Figure S.13.)). These sensors could be re-used, giving a reproducible response towards Cl^-. Such reproducibility could be observed through the hysteresis test (Figure S.14.). In this case, the sensors were immersed inside a solution containing 1 mM NaCl. This solution was then changed to a less concentrated NaCl solution containing 10 µM. The devices were finally immersed again inside the concentrated solution. In both cases, when the devices were immersed inside the concentrated NaCl solution, a similar potentiometric signal, in the range of -107 mV was achieved, indicating a good reproducibility of the devices. This reproducibility of the measurements was additionally proven using 3 different chlorinated

salts. The ion sensor showed a similar response when measuring chloride ions from NaCl, KCl and $CaCl_2$ as shown in Figure 4.d). Additionally, the ion sensing device showed an unprecedented selectivity towards chloride ions when compared to other halogens such as F^-, Br^- and anions like SO_4^{2-}, NO_3^-, and HCO_3^-. These electrolytes were specifically tested due to their essential roles in the clinical diagnostic for diseases resulted from electrolytes imbalance[62-64].

A significant reduction in sensitivity of the sensing films was observed when non-chlorinated salts were employed. F- represented the main interference electrolyte, since the sensors showed a sensitivity of -70±23 mV.Log$[F^-]^{-1}$ to this anion, being almost 3 times lower than the sensitivity towards Cl^-. In addition, the sensitivity towards Br^- and SO_4^{2-} ions was about 5 times lower than the sensitivity towards Cl^-, with -43±6 mV.Log$[Br^-]^{-1}$ and -40±7 mV.Log$[SO_4^{2-}]^{-1}$, respectively. However, the sensor only showed these sensitivity levels at concentrations higher than 40 mM for the main interference electrolytes. Given the low concentration ranges of these anions under physiological conditions (in most cases lower than 40 mM), the level of interference of these anions is expected to be low. A negligible sensitivity value towards nitrate, carbonate and hydroxyl ions were also observed, with -28±11, -10±20, and -8±3 mV.Log$[C^-]^{-1}$, respectively. However, in the case of OH^-, due to the solubility of the silica compounds in the presence of a high pH, the sensors could only be assessed in a concentration of up to 10^{-2} M. The reported selectivity represents a significant enhancement in sensitivity towards chloride ion by at least 3-fold when compared with the currently available commercial technologies for chloride ions detection.

The sensing devices showed selectivity towards chloride in solutions containing a mixture of interfering ions, including the above-mentioned F^-, Br^-, SO_4^{2-}, NO_3^- and HCO_3^-. These interfering ions did not significantly change the OCP signal of the devices when 10 mM of each ions were included simultaneously in the tested solution (Figure 4.e). The sensors could raise a super-Nernst signal even when high concentrations of interference analytes as shown in Figure S.15. In this case, 0.1 M of each interfering ion (SO_4^{2-}, Br^-, F^-, HCO_3^-) was used. No significant decrease in OCP was obtained when these ions were incorporated inside the solution. Only when 0.1 M of NaF, a decrease of -18 mV was observed. On the contrary, upon addition of 1 mM NaCl, the potentiometric signal of the sensors decreased by -138 mV, being close to the expected decrease of -186 mV due to the super-Nernst nature of the sensors. The lower signal change reported in this case was a consequence to the high concentration of

interferences, which could reduce the sensitivity of the gold/silica nanoparticles. However, this effect was only observed when large concentration of interferences were used. As such, it is not expected to significantly hinder the sensitivity of the sensors when used in biological solutions.

As such, the selectivity of the devices was demonstrated. This selectivity was also evaluated by calculating the selectivity coefficient of the silica/gold ionically imprinted nanoparticles using the matched potential method. The selectivity towards similar anions including F^- and Br^- was $k_{Cl,F}^{MPM}$ = -2.1 and $k_{Cl,Br}^{MPM}$ = -2.0, being superior to the previously reported work in the literature using neutral ionophores[65], which is in the range of +0.2 for Br^-. A complete list of selectivity for the studied anions is provided in Table S.1.

The normal concentration of chloride in human serum is between 96-106 mM[66]. Chloride ion imbalances are associated with multiple conditions such as kidney disease, heart failure, and high chloride concentrations are observed in about 25-45% of intensive care unit patients[67], with abnormal concentrations being related to the severity of the pathology[68]. In particular, the concentration of chloride in serum are associated with a higher risk of death and cardiovascular complications within patients with chronic kidney disease[69]. However, the continuous monitoring of chloride can be challenging due to the lack of selective sensors that can be adapted for their real-time determination. Moreover, the early detection of these complications due to chloride ions cannot be accomplished by the measurement of serum or dialysate pH alone, due to the presence of buffering systems to stabilize the acidity within physiological levels.

The high sensitivity and selectivity of the chloride ion sensors described here allowed its use in a clinical environment, for the determination of chloride extraction from dialysate samples, collected from patients with chronic kidney disease (Figure 4.f). These dialysate samples were the result of filtrating the blood of patients using a dialysate solution to regulate the concentration of electrolytes. Initially, the chloride sensing devices were tested in commercially available human serum, and the concentration was measured. The serum sample was then spiked with 10 mM NaCl to increase the concentration of Cl^-. The final device could accurately determine the concentrations of chloride ions in pristine serum, and serum obtained after spiking using 10 mM NaCl. The obtained concentrations were within the range of standard value of human serum, demonstrating the suitability of this device in diagnosis (Figure S.16).

A sensing device was then fabricated by using a scree-printed electrode, consisting of a Ag/AgCl reference, and a carbon-based working and counter electrodes. The working electrode was first modified by depositing a thin (50 nm) film, and the Silica/Gold ionically imprinted nanoparticles were deposited following the previously reported method (Figure S.17.a.). The final device achieved a sensitivity of 177.3 mV/Log[Cl^-], and a detection limit in the range of 10^{-3} M (Figure S.17.b.). Dialysate samples were taken from 3 patients at different times during the dialysis process (5, 15, 30, 60 and 120 mins), and the chloride concentration was determined. In all cases, a decrease in the measured chloride concentrations after 2 h of dialysis compared to the initial values was recorded. This result is consistent with the active filtration of chloride from the patients within the dialysis setup. The measured concentration decreased to 85±1, 76±10, and 94.1±0.2 mM after 2 hours. Only in one case, the measured concentration lied within the standard clinical values. In the case of patients 1 and 2, the final concentrations were significantly lower than the standard values. These result evidence the need of a monitoring device for the determination of chloride concentrations in patients, which would allow a modulation of the chloride concentrations being filtered. The device would decrease the hypochloremia rates within patients undergoing haemodialysis.

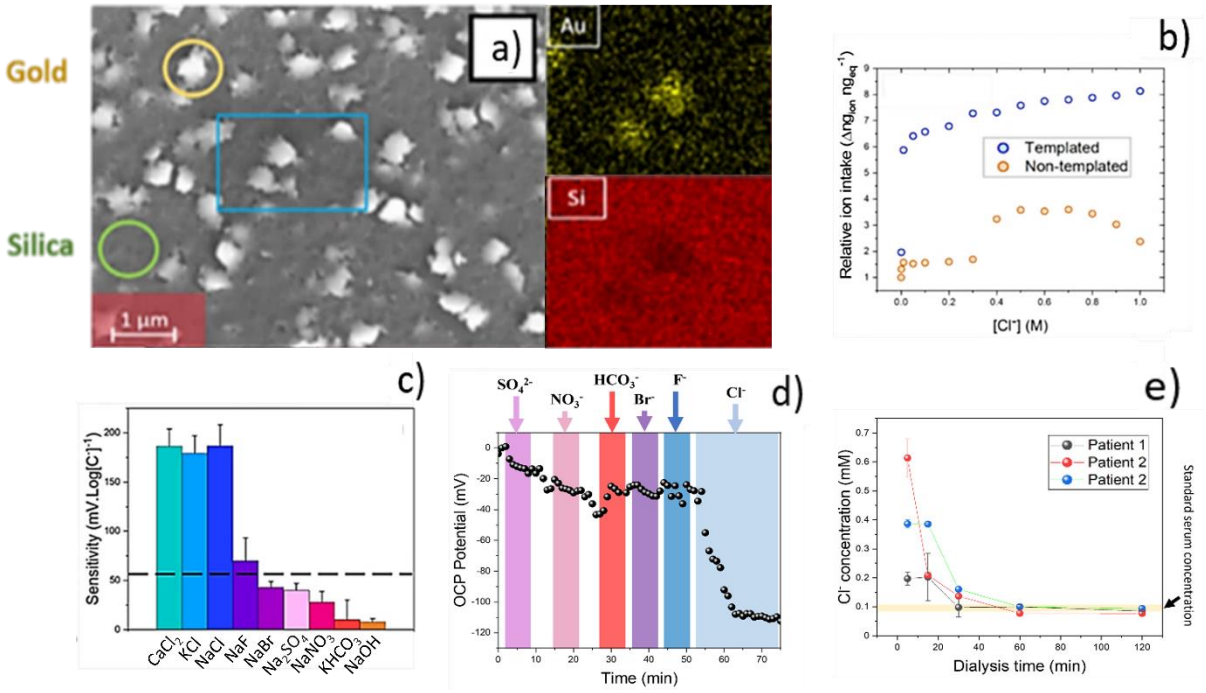

Figure 4. a) SEM image of the sensing film containing the ion imprinted silica/gold nanoparticulate surface morphology. The EDS elemental mapping of gold and silica in the highlighted area is also shown. **b)** Relative absorption of chloride ions by the ion-imprinted electrodes grafted onto gold surfaces as measured by quartz microbalance. These values were measured by subjecting the film to different concentrations of NaCl, and the results were normalized by the first observed weight value, when only water was used. c**)** Sensitivity profiles of the ionic imprinting-based electrodes after testing with different metal chlorides (NaCl, KCl, $CaCl_2$) and interference anions from Na_2SO_3, $NaNO_3$ and $KHCO_3$. **d)** Monitoring of the OCP signal of a sensing device containing the gold/silica ionically imprinted nanoparticles when subjected to a mixed concentration of anions. The result of cumulatively adding 10 mM SO_4^{2-} (grey), 10 mM of NO^{3-} (blue), 10 mM HCO_3^- (green), 10 mM Br^- (pink) and 10 mM F^- (orange) was measured. Only a significant change in the potentiometric signal can be observed when Cl^- is added. e**)** Measured concentrations of chloride in dialysate samples of 3 patients. Samples were taken at 5 different times (5, 15, 30, 60, 120 min), and the standard concentration of chloride in human serum is indicated. The standard range of chloride concentration in human serum (96-106 mEq/L) is also indicated.

The amount of template ions (Cl^-) employed during the synthesis of the ion imprinted silica/gold nanoparticles played a crucial role in the performance of the final device. Since Cl^- was used for the creation of a specific pore by its interaction with the aminated APTES

molecules, its concentration and stoichiometry with respect to APTES had to be tightly regulated to ensure a homogeneous formation of the specific pores. This fact was demonstrated using different amounts of HCl during the synthesis of the ion imprinted silica/gold nanoparticles while keeping the amount of APTES constant and measuring the sensitivity of the devices. When small concentrations of the HCl template was employed, in the range of 0.5 mM, a low sensitivity of -17.4 mV.Log$[Cl^-]^{-1}$ was obtained. This sensitivity was over 10 times lower than the sensitivity achieved in the present work using 1 mM of HCl, which is in the range of -186.4 mV.Log$[Cl^-]^{-1}$. Such a low sensitivity was attributed to the low availability of the Cl^- templates, leading to the formation of non-specific domains on the surface of the nanoparticles since there are APTES molecules that do not interact with the Cl^- templates, and a low degree of quaternisation of such APTES molecules. On the contrary, when higher amounts of HCl were employed, the sensitivity was still suboptimal, with -99.1 mV.Log$[Cl^-]^{-1}$. Although this sensitivity was higher than the one achieved when low amounts of HCl template were employed, it was significantly lower than the optimal sensitivity at 1 mM HCl. Under optimal conditions, the chloride ions were adsorbed by a combination of electrostatic interactions and hydrogen bonds[31]. However, when high concentrations of template were used compared to APTES, the pores did not present the optimal conditions for such interactions. Consequently, the sensitivity of the devices was reduced (Figure S.18).

Conclusions

We have demonstrated for the first time the application of ionically imprinted nanomaterials in the form of ultra-thin (e.g. 300 nm thick) nanostructured films with silica/gold core-shell nanoparticles as sensing element for the detection of Cl^-. The device exhibited a superior sensitivity of -186.4 mV.Log$[C^-]^{-1}$. This sensitivity surpassed the limit of the current state-of-the-art chloride ion-selective electrodes, which tend to have a thermodynamical limit of 59 mV.Log$[C^-]^{-1}$ under Open-Circuit potential measurements and tend to have a relatively thick sensing layer (typically above 100 μm). Therefore, the novel anion sensing device developed here exhibited a 3-fold higher sensitivity, with a detection limit in the range of 10^{-4} M. These sensors were proven to offer a stable signal, with a low drift in the range of 1.1 mV h^{-1} and did not require the current lengthy and laborious pre-conditioning process in the commercial anion sensing devices. Such a significant enhancement was possible due to the adsorption of the electrolytes to the specific surface interactions with the ion imprinted nanopores on the silica/gold core-shell nanoparticles and the use of positively charged functional groups. The surfaces interactions also provided a high selectivity to the devices,

surpassing the one reported by using ionophores. This proposed new sensing mechanism based on the adsorption of ions on the silica/gold core-shell nanoparticles has enabled the miniaturization and fabrication of fully functional ultra-thin sensing films with sub-micrometer dimensions, which is not possible using the current commercial plasticized PVC technology which relying on the bulk diffusion of ions inside the sensing films. These anion sensors also showed an unprecedented selectivity towards chloride ions, as demonstrated by calibrating the response of the sensors towards some of the most common interferences found in these sensors, including HCO_3^-, NO_3^- and SO_4^{2-}. In addition, they remained stable up to a pH of 11. The device also demonstrated the capability and suitability in diagnosis as evidenced by the detection of chloride ions in pristine serum, and serum obtained after spiking using 10 mM NaCl (i.e. within the range of standard value of human serum). This breakthrough would open up the opportunity to the fabrication of tailor-made nanostructured thin films for the selective detection of challenging ionic species, especially anions with high specificity and selectivity, which is critical for a wide range of currently important technologies, including environmental remediation, drug development and energy storage among others. The sensing performance could potentially be enhanced in the future through the incorporation of nanomaterials with a positively charged surface, instead of the negatively charged silica. Nanomaterials such as microporous zeolites or porous metallic nanoparticles could be potentially incorporated to enhance the electrostatic attractions between the negatively charged anions and the sensing particles, and potentially avoid the need for the incorporation of expensive metallic components (i.e. gold nanoparticles).

Finally, the material presented in this work, shows the potential to be modified, to enable the detection of other anions, not restricted to halides. Changes in the selectivity of the nanoparticles could potentially be achieved by changing the template ion within the synthesis process, and tailoring the concentration of interacting functional groups (i.e. amines), which could lead to different pore sizes on the silica nanoparticles. Similar strategies have been adopted in the design of ionophores for halide detection using cyclic molecules such as crown ethers.

Experimental Section

Materials

Tetraethyl orthosilicate (TEOS), tetra chloroauric acid, citric acid, 3-aminopropyl trimethoxysilane (APTES), 1-Ethyl-3-(3-dimethylaminopropyl) carbodiimide, N-hydroxysuccinimide (NHS), Dimethyl formamide, 16-mercaptohexadecanoic acid, sodium chloride, calcium chloride, potassium chloride, sodium sulfate, potassium carbonate, human serum, sodium nitrate and hydrochloric acid were purchased from Sigma Aldrich. All the chemicals were used at HPLC grade unless indicated.

Fabrication of thin film conducting electrode

A 50 nm thin gold film was deposited onto a glass substrate by plasma sputtering (Q150RES, Quorum technologies, UK) using standard conditions. Here, a methacrylate mask was first pre-fabricated using a laser cutter (PLS6.75, Universal Laser Systems, Austria). This mask was designed for the deposition of up to 5 electrodes after positioning them onto 7.5x2.5 cm glass slides and subsequently to be sputtered with gold. Each individual electrode had a radius of 5 mm.

Gold NP synthesis

The ionically imprinted material consisted of a gold nanocluster aggregate integrated with a nanoporous silica shell. These gold nanoparticles were synthesized by the reduction of tetrachloroauric acid (TCA) with citric acid as reported elsewhere[70]. Briefly, a 5 mL solution of 5 mM TCA was mixed in 90 mL of DI water under constant stirring and heated up to 80 ^{o}C. Citric acid 0.5% in 5 mL was then added and incubated for 6 h until a red-colored solution was obtained, indicating the success of the synthesis of Au nanoparticles.

Nanoporous core-shell Silica-Au by nanoimprinting

Nanoporous ion Imprinted silica nanoparticles were synthesized by mixing 4 mM of APTES and 20 mM of TEOS in an aqueous solution containing 10 mL of 1:1 ethanol:water. A concentration of 1 mM HCl was used to provide the Cl- ionic template while providing an acidic environment, favoring the quaternization of aminated species (Figure 5.b). A volume of 5 mL of the gold nanoparticle dispersion was then mixed with this solution, and the final mixture was incubated overnight at 4 ^{o}C. The synthesized nanoparticles were washed twice using DI water and dispersed in DMF. A non-templated control sample was additionally synthesized by a similar approach without using HCl.

Sensing device fabrication

The fabrication steps and procedures of the sensing materials and device are summarized in Figure 5 and the details are presented below. A self-assembled monolayer of thiolated polycarbons was functionalized onto the gold electrodes by immersing a solution of 1 mM in ethanol overnight (Figure 5.d). APTES was then directionally grafted using standard EDC/NHS chemistry (Figure 5.e). A solution of 15 mM of APTES amine was mixed with the EDC. A volume of 1 mL of a DMF solution containing NHS using a ratio of 1:2 of EDC:NHS, was then used onto the gold electrode and was incubated for at least 5 mins. The EDC-containing solution was dropped onto the electrodes and they were incubated for at least 4 h. After grafting, the sensor was washed twice by immersing in a solution a mixture of 1:1 ethanol and water to remove any residuals of the EDC and NHS reagents, and the porous core-shell of silica/Au nanoparticulate dispersion was applied to the functionalized electrode in order to induce the nanoparticle grafting and linking of the silica/Au nanoparticulate dispersion.

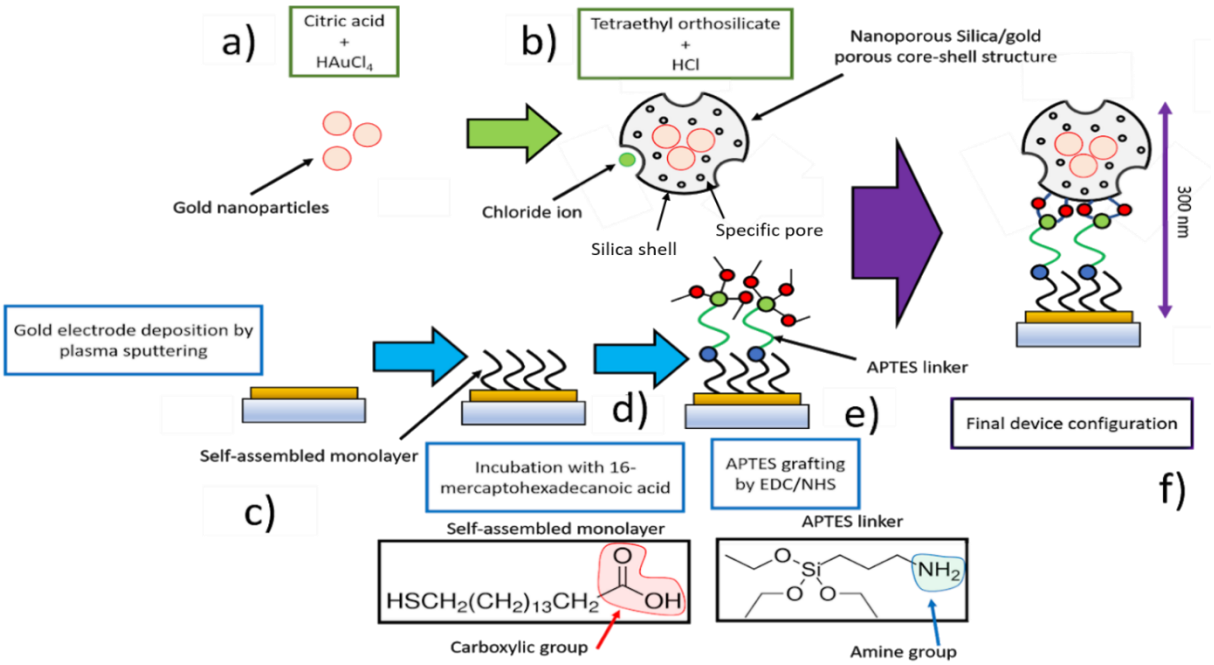

Figure 5. a) Gold NPs synthesis: Au nanoclusters were first synthesized using citric acid as the reducing agent in the presence of $HAuCl_4$. **b)** Microporous core shell Silica/Au nanoparticles via ionic imprinting method for selective Cl^- sensing: The ionically-imprinted imprinted outer silica shell is synthesized using tetraethyl orthosilicate as the structural units and HCl as the template, using APTES to favor the interaction with the chloride ions. APTES is positively charged in the presence of an acid environment as generated by the HCl, increasing the interaction between the porous nanoparticles and the chloride ions. A microporous nanoparticle silica/Au with controlled porosity (circa. 1.5 nm in pore size) specific towards chloride ions is then developed. **c)** Electrode fabrication: In parallel, 50 nm thick gold conducting film was deposited onto glass substrate by plasma sputtering. **d)** Functionalization of Au electrode: This is achieved by introducing a self-assembled monolayer of 16-mercaptohexadecanoic acid, containing a -SH group that can strongly bind to the gold film, and a carboxyl group(-COOH). **e)** Linkages: The free -COOH group of the functionalized Au electrode in d) was used to guide the directional attachment of the APTES linker that bridge the electrode with the siloxane groups on the core shell silica-gold synthesized in b) in order to produce f) via the use standard EDC/NHS chemistry; **f)** A 300 nm thick nanostructured sensing film is finally produced specific for the detection of chloride ions.

Structural characterization of the sensing layers

The morphology of the synthesized silica/Au nanoparticles synthesized by ion imprinting was characterized using Scanning Electron Microscopy (SEM) (EVO LS15, ZEISS, Germany). High resolution transmission electron microscopy (HRTEM) images of the nanoparticles were also taken using a field emission gun transmission electron microscope (FEG-TEM, JEM-2100F, JEOL, Japan) operated at the accelerating voltage of 200 kV. The high-angle annular dark-field imaging-Scanning transmission electron microscope (HAADF-STEM) image was obtained with an Annular Dark Field (ADF) detector attached to the TEM at a camera length of 8 cm. Stylus profilometer (Dektakxt, Bruker, UK) was also used to determine the thickness of the as-fabricated sensing layer in Figure 5.f).

Chemical analysis and composition characterization of the sensing layers

Chemical analysis was performed using FTIR (L160000A Perkin Elmer, US) and EDS mapping of the elemental composition was carried out on the sensing layers. The surface area and pore size distribution of the ion imprinted silica/Au nanoparticles were determined using BET Surface analyzer (Quantachrome, NOVATouch, UK). XPS was carried out using a Thermo K-alpha spectrometer equipped with a monochromated Al K-Alpha X-ray source (1486.6 eV) in constant analyser energy mode. A pass energy of 200 eV was used to record survey spectra, and 50 eV was used to record the core level spectra, with a 400 μm diameter spot size. Sample charging was prevented by use of a dual beam flood gun. The binding energy scale was calibrated to the C 1s, C*-C/C*-H aliphatic peak at 284.8 eV. Curve fitting of narrow scan spectra was performed using the processing software CasaXPS.1 The peak components were modelled, after Shirley background subtraction, by a convolution of Gaussian (70 %) and Lorentzian (30 %) functions. The full widths at half-maximum (fwhm) were constrained to be equal for component peaks within each spectrum.

Sensing performance characterization

The relative ion intake of the sensing device in Figure 5.f) was determined using a quartz microbalance (Q-sense, Biolin Scientific, Switzerland), and compared to the non-templated control samples (without including HCl in the precursor solution). The electrochemical analysis and sensing performance was carried out by measuring the Open Circuit Potential (OCP) of the sensors upon being subjected to different solutions with anions Cl^-, SO_4^{2-}, NO_3^-, HCO_3^- at different concentrations (10^{-4}, 10^{-3}, 10^{-1}, 1, 10, 40, 80 and 160 mM) and studying the specificity towards interference ions using a standard 3-electrode configuration, with a

Ag/AgCl reference and a platinum counter electrode. The sensitivity of the electrodes towards Cl^- was also repeated by using imprinted nanoparticles with no gold nanoparticles as the core material. The selectivity of the devices was determined by using the matching potentials method. As a verification of the selectivity, the OCP potential of the sensors was recorded while concentrations of 10 mM of the different anions here employed were added.
For the determination of the effects of pH on the sensing performance, NaOH and H_2SO_4 were added to DI water to change the pH values. 5 different pH were tested (3, 5, 7, 9 and 11), and the sensitivity of the devices using NaCl solutions at the concentrations above mentioned was determined.
The sensing devices were also tested under a clinical setup in an observational pilot study (approved by UK National Research Ethics committee, 21-NI-0059), by measuring the concentration of chloride within dialysate samples in 3 adult patients with chronic kidney disease attending for routine outpatient haemodialysis treatments. Informed consent was obtained prior the research. In this case, dialysate samples collected from the waste output of a haemodialysis filtration system were collected at 5 different times (5, 15, 30, 60 and 120 mins). A sensing device consisting of a screen-printed electrode where the working sensor area had been modified through the deposition of a thin (50 nm) gold film was fabricated. The devices were first calibrated using different concentrations of NaCl, and they were immersed in the dialysate samples directly. The changes in the OCP signal could be directly correlated with the Cl^- concentration.

References

1. Desai, A.S., Swedberg, K., McMurray, J.V., Granger C., Yusuf S., Young, J.B., Dunlap, M.E., Solomon, S.D., Hainer, J.W., Olofsson B., Michelson E.L., Pfeffer, M.A. Incidence and Predictors of Hyperkalemia in Patients With Heart Failure: An Analysis of the CHARM Program. Journal of the American College of Cardiology, 2007. 50(20): p. 1959-1966.
2. Sica, D.A. Deterrent to the Use of Aldosterone Receptor Antagonism or Not. Hypertension, 2009. 53(5): p. 749-750.
3. Gao, W., Emaminejad S., Nyein, H.Y., Challa, S., Chen, K., Peck, A., Fahad, H.M., Ota, H., Shiraki, H., Kiriya, D., Lien, D., Brooks, G.A., Davis, R.W., Javey, A. Fully integrated wearable sensor arrays for multiplexed in situ perspiration analysis. Nature, 2016. 529(7587): p. 509-514.
4. Lin, W.C., Li, Z., Burns., M.A. A Drinking Water Sensor for Lead and Other Heavy Metals. Analytical Chemistry, 2017. 89(17): p. 8748-8756.

5. Chen, F., Z.Y. Leong, and H.Y. Yang. An aqueous rechargeable chloride ion battery. Energy Storage Materials, 2017. 7: p. 189-194.
6. Song, Y., Jiang, G., Chen, Y., Zhao, P., Tian, Y. Effects of chloride ions on corrosion of ductile iron and carbon steel in soil environments. Scientific Reports, 2017. 7(1): p. 686.
7. Adamchuk, V.I., Hummel, J. W., Morgan, M.T., Upadhyaya S.K. On-the-go soil sensors for precision agriculture. Computers and Electronics in Agriculture, 2004. 44(1): p. 71-91.
8. Luke, R.G. Serum Chloride and Bicarbonate Levels in Chronic Renal Failure. Archives of Internal Medicine, 1979. 139(10): p. 1091-1092.
9. Neligan, P.J., O'Donoghue R. How Should Acid-Base Disorders Be Diagnosed and Managed?, in Evidence-Based Practice of Critical Care, C.S. Deutschman and P.J. Neligan, Editors. 2010, W.B. Saunders: Philadelphia. p. 389-396.
10. Winkler, S., Rieger, L., Pressl, A., Gruber, G. Application of ion-sensitive sensors in water quality monitoring. Water science and technology. Journal of the International Association on Water Pollution Research, 2004. 50: p. 105-14.
11. Heller, L., M. Ben-Yair. Effect of chloride solutions on portland cement. Journal of Applied Chemistry, 1966. 16(8): p. 223-226.
12. Gemene, K.L., Meyerhoff, M.E. Selectivity Enhancement for Chloride Ion by In(III)-Porphyrin-Based Polymeric Membrane Electrode Operated in Pulsed Chronopotentiometric Mode. Electroanalysis, 2012. 24(3): p. 643-648.
13. Lewenstam, A. Routines and Challenges in Clinical Application of Electrochemical Ion-Sensors. Electroanalysis, 2014. 26(6): p. 1171-1181.
14. Ryoichi Ishimatsu, Anahita Izadyar, Benjamin Kabagambe, Yushin Kim, Jiyeon Kim, and Shigeru Amemiya. Electrochemical Mechanism of Ion–Ionophore Recognition at Plasticized Polymer Membrane/Water Interfaces. Journal of the American Chemical Society, 2011. 133(40): p. 16300-16308.
15. Jarolímová, Z., Han, T., Mattinen, U., Bobacka, J., Bakker, E. Capacitive Model for Coulometric Readout of Ion-Selective Electrodes. Analytical Chemistry, 2018. 90(14): p. 8700-8707.
16. Zdrachek, E., Bakker, E. Potentiometric Sensing. Analytical Chemistry, 2019. 91(1): p. 2-26.
17. Schaller, U., E. Bakker, Pretsch, E. Carrier mechanism of acidic ionophores in solvent polymeric membrane ion-selective electrodes. Analytical Chemistry, 1995. 67(18): p. 3123-3132.

18. Bakker, E. Enhancing ion-selective polymeric membrane electrodes by instrumental control. TrAC Trends in Analytical Chemistry, 2014. 53: p. 98-105.
19. Szigeti, Z., Vigassy, T., Bakker, E., Pretsch, E. Approaches to Improving the Lower Detection Limit of Polymeric Membrane Ion-Selective Electrodes. Electroanalysis, 2006. 18(13-14): p. 1254-1265.
20. Keplinger, F., Glatz, R., Jachimowicz, A., Urban, G., Kohl, F., Olcaytug, F., Prohaska, O.J. Thin-film ion-selective sensors based on neutral carrier membranes. Sensors and Actuators B: Chemical, 1990. 1(1): p. 272-274.
21. Sanggil, H., Yamamoto, S., Polyravas, A., Malliaras, G. Microfabricated Ion-Selective Transistors with Fast and Super-Nernstian Response. Advanced Materials. 2020. p. 2004790
22. Raimondo, J. V., Burman, R. J., Katz, A.A., Akerman, C. J. Ion dynamics during seizures. Front. Cell. Neurosci. 2015, 9, 419.
23. Rothberg, J. M., Hinz, W., Rearick, T. M., Schultz, J., Mileski, W., Davey, M., Leamon, J. H., Johnson, K., Milgrew, M. J., Edwards, M., Hoon, J., Simons, J. F., Marran, D., Myers, J. W., Davidson, J. F., Branting, A., Nobile, J. R., Puc, B. P., Light, D., Clark, T. A., Huber, M., Branciforte, J. T., Stoner, I. B., Cawley, S. E., Lyons, M., Fu, Y., Homer, N., Sedova, M., Miao, X., Reed, B., Sabina, J., Feierstein, E., Schorn, M., Alanjary, M., Dimalanta, E., Dressman, D., Kasinskas, R., Sokolsky, T., Fidanza, J. A., Namsaraev, E., McKernan, K. J., Williams, A., Roth, G. T., Bustillo, J. An integrated semiconductor device enabling non-optical genome sequencing. Nature 2011, 475, 348.
24. Shklovskii, B.I. Screening of a macroion by multivalent ions: Correlation-induced inversion of charge. Physical Review E, 1999. 60(5): p. 5802-5811.
25. Grosberg, A.Y., Nguyen, T.T., Shklovskii, B.I. Colloquium: The physics of charge inversion in chemical and biological systems. Reviews of Modern Physics, 2002. 74(2): p. 329-345.
26. Sivakumarasamy, R., Hartkamp, R., Siboulet, B., Dufrêche, J.F., Nishiguchi, K., Fujiwara, A., Clément, N. Selective layer-free blood serum ionogram based on ion-specific interactions with a nanotransistor. Nature Materials, 2018. 17(5): p. 464-470.
27. Abdelwahab, O., Amin, N.K., El-Ashtoukhy, E.S.Z. Removal of zinc ions from aqueous solution using a cation exchange resin. Chemical Engineering Research and Design, 2013. 91(1): p. 165-173.
28. Koivula, R., Lehto, J., Pajo, L., Gale, T., Leinonen H. Purification of metal plating rinse waters with chelating ion exchangers. Hydrometallurgy, 2000. 56(1): p. 93-108.

29. Rivas, B. L., Maturana, H. A., Villegas, S., Pereira, E. Interaction of heavy metal ions with an ion exchange resin obtained from a natural polyelectrolyte. Polymer Bulletin, 1998. 40(6): p. 721-728.
30. Dudzinska, M.R., Clifford, D.A. Anion exchange studies of lead-EDTA complexes. Reactive Polymers, 1991. 16(1): p. 71-80.
31. Chen, H., et al., Hierarchically Molecular Imprinted Porous Particles for Biomimetic Kidney Cleaning. 2020. 32(52): p. 2005394.
32. Fu, J., Chen, L., Lia, J., Zhang, Z. Current status and challenges of ion imprinting. Journal of Materials Chemistry A, 2015. 3(26): p. 13598-13627.
33. Branger, C., Meouche, W., Margaillan, A. Recent advances on ion-imprinted polymers. Reactive and Functional Polymers, 2013. 73(6): p. 859-875.
34. Dakova, I., Karadjova, I., Ivanov, I., Georgieva, V., Evtimova, B., Georgiev, G. Solid phase selective separation and preconcentration of Cu(II) by Cu(II)-imprinted polymethacrylic microbeads. Analytica Chimica Acta, 2007. 584(1): p. 196-203.
35. Yılmaz, V., Hazer, O., Kartal, Ş. Synthesis, characterization and application of a novel ion-imprinted polymer for selective solid phase extraction of copper(II) ions from high salt matrices prior to its determination by FAAS. Talanta, 2013. 116: p. 322-329.
36. Dam, H.A., Kim, D. Selective Copper(II) Sorption Behavior of Surface-Imprinted Core−Shell-Type Polymethacrylate Microspheres. Industrial & Engineering Chemistry Research, 2009. 48(12): p. 5679-5685.
37. Zhang, N., Hu, B. Cadmium (II) imprinted 3-mercaptopropyltrimethoxysilane coated stir bar for selective extraction of trace cadmium from environmental water samples followed by inductively coupled plasma mass spectrometry detection. Analytica Chimica Acta, 2012. 723: p. 54-60.
38. Behbahani, M., Barati, M., Bojdi, M.K., Pourali, A.R., Bagheri, A., Tapeh, N.A.G. A nanosized cadmium(II)-imprinted polymer for use in selective trace determination of cadmium in complex matrices. Microchimica Acta, 2013. 180(11): p. 1117-1125.
39. Wang, Z., Wu, G., He, C. Ion-imprinted thiol-functionalized silica gel sorbent for selective separation of mercury ions. Microchimica Acta, 2009. 165(1): p. 151-157.
40. Zhu, X., Cui, Y., Chang, X., Zou, X., Li, Z. A surface ion-imprinted mesoporous sorbent for separation and determination of Pb(II) ion by flame atomic absorption spectrometry. Microchimica Acta, 2009. 164(1): p. 125-132.

41. Jenkins, A.L., Uy, O.M., Murray, G.M. Polymer-Based Lanthanide Luminescent Sensor for Detection of the Hydrolysis Product of the Nerve Agent Soman in Water. Analytical Chemistry, 1999. 71(2): p. 373-378.
42. Carrasco, S., et al., Multibranched Gold–Mesoporous Silica Nanoparticles Coated with a Molecularly Imprinted Polymer for Label-Free Antibiotic Surface-Enhanced Raman Scattering Analysis. Chemistry of Materials, 2016. 28(21): p. 7947-7954.
43. Xie, C., et al., Molecular Imprinting at Walls of Silica Nanotubes for TNT Recognition. Analytical Chemistry, 2008. 80(2): p. 437-443.
44. Kala, R., Rao, T.P. Ion imprinted polymer particles for separation of yttrium from selected lanthanides. Journal of Separation Science, 2006. 29(9): p. 1281-1287.
45. Bomar, E.M., Owens, G.S., Murray, G.M. Nitrate Ion Selective Electrode Based on Ion Imprinted Poly(N-methylpyrrole). Chemosensors, 2017. 5(1): p. 2.
46. Alizadeh, T., Atayi, K. Synthesis of hydrogen phosphate anion-imprinted polymer via emulsion polymerization and its use as the recognition element of graphene/graphite paste potentiometric electrode. Materials Chemistry and Physics, 2018. 209: p. 180-187.
47. Laurinavichyute, V.K., Nizamov, S., Mirsky, V.M. The Role of Anion Adsorption in the Effect of Electrode Potential on Surface Plasmon Resonance Response. Chem. Phys. Chem, 2017. 18(12): p. 1552-1560.
48. Bradbury, C.R., Zhao, J., Fermín, D.J. Distance-Independent Charge-Transfer Resistance at Gold Electrodes Modified by Thiol Monolayers and Metal Nanoparticles. The Journal of Physical Chemistry C, 2008. 112(27): p. 10153-10160.
49. Kang, C., Li, W., Tan, L, Li, H., Weic, C., Tang, Y. Highly ordered metal ion imprinted mesoporous silica
particles exhibiting specific recognition and fast adsorption kinetics. Journal of Materials Chemistry A, 2013. 1(24): p. 7147-7153.
50. Zhang, Z., Zhang, X., Niu, D., Li, Y., Shi, J. Highly efficient and selective removal of trace lead from aqueous solutions by hollow mesoporous silica loaded with molecularly imprinted polymers. Journal of Hazardous Materials, 2017. 328: p. 160-169.
51. Yang, S., Qian, J., Kuang, L., Hua, D. Ion-Imprinted Mesoporous Silica for Selective Removal of Uranium from Highly Acidic and Radioactive Effluent. ACS Applied Materials & Interfaces, 2017. 9(34): p. 29337-29344.
52. Kamra, T., Chaudhary, S., Xu, C., Montelius, L., Schnadt, J., Ye, L. Covalent immobilization of molecularly imprinted polymer nanoparticles on a gold surface using

carbodiimide coupling for chemical sensing. Journal of Colloid and Interface Science, 2016. 461: p. 1-8.

53. R. A. Shircliff, P. Stradins, H. Moutinho, J. Fennell, M. L. Ghirardi, S. W. Cowley, H. M. Branz and I. T. Martin, Langmuir, 2013, 29, 4057-4067.

54. S. M. Scholz and K. Jacobi, Surface Science, 1996, 369, 117-125.

55. E. H. Williams, J. A. Schreifels, M. V. Rao, A. V. Davydov, V. P. Oleshko, N. J. Lin, K. L. Steffens, S. Krylyuk, K. A. Bertness, A. K. Manocchi and Y. Koshka, Journal of Materials Research, 2013, 28, 68-77.

56. Zhang, D., Hegab, H.E., Lvov, Y., Snow, L.D., Palmer, J. Immobilization of cellulase on a silica gel substrate modified using a 3-APTES self-assembled monolayer. SpringerPlus, 2016. 5(1): p. 48-48.

57. Li, Y., Liu, Y., Liu, J., Liu, J., Tang, H., Cao, C., Zhao, D., Ding, Y. Molecularly imprinted polymer decorated nanoporous gold for highly selective and sensitive electrochemical sensors. Scientific Reports. 2014.

58. Hamza, M. Grafting of quaternary ammonium groups for uranium(VI) recovery: application on natural acidic leaching liquor. Journal of Radioanalytical and Nuclear Chemistry, 2019. 1-14.

59. Coll Crespi, M., et al., Agarose hydrogel containing immobilized pH buffer microemulsion without increasing permselectivity. Talanta, 2018. 177: p. 191-196.

60. Guzinski, M., Jarvis, J.M., Pendley, B.D., Lindner, E. Equilibration Time of Solid Contact Ion-Selective Electrodes. Analytical Chemistry, 2015. 87(13): p. 6654-6659.

61. Wang, C., Yuan, H., Duan, Z., Xiao, D. Integrated multi-ISE arrays with improved sensitivity, accuracy and precision. Scientific Reports, 2017. 7(1): p. 44771.

62. Brunetti, M., Terracina, L., Timio, M., Saronio, P., Capodicasa, E. Plasma sulfate concentration and hyperhomocysteinemia in hemodialysis patients. Journal of nephrology, 2001. 14: p. 27-31.

63. Miller, G.D., Marsh, A.P., Dove, R.W., Beavers, D., Presley, T., Helms, C., Bechtold, E., Bruce King, S., Kim-Shapiro, D. Plasma nitrate and nitrite are increased by a high nitrate supplement, but not by high nitrate foods in older adults. Nutrition Research, 2012. 32(3): p. 160-168.

64. Basile, C., L. Rossi, Lomonte, C. The choice of dialysate bicarbonate: do different concentrations make a difference? Kidney International, 2016. 89(5): p. 1008-1015.

65. Y. Su, S. Xia, R. Wang, L. Xiao. Hormone Metabolism and Signaling in Plants ,2017. 431-470.

66. Pfortmueller, C.A., Uehlinger, D., von Haehling, S., Schefold, J.C. Serum chloride levels in critical illness—the hidden story. Intensive care medicine experimental, 2018. 6(1): p. 10-10.
67. Marttinen, M., Wilkman, E., Petaja, L., Suojaranta-Ylinen, R., Pettila, V., Vaara, S.T. Association of plasma chloride values with acute kidney injury in the critically ill - a prospective observational study. Acta Anaesthesiol Scand, 2016. 60(6): p. 790-9.
68. Berend, K., van Hulsteijn, L.H., Gans, R.O. Chloride: the queen of electrolytes? Eur J Intern Med, 2012. 23(3): p. 203-11.
69. Kubota, K., Sakaguchi, Y., Hamano, T., Oka, T., Yamaguchi, S., Shimada, K., Matsumoto, A., Hashimoto, A., Mori, D., Matsui, I., Isaka, Y. Prognostic value of hypochloremia versus hyponatremia among patients with chronic kidney disease—a retrospective cohort study. Nephrology Dialysis Transplantation, 2018. 35(6): p. 987-994.
70. Dar, A.I., Walia, S., Acharya, A. Citric acid-coated gold nanoparticles for visual colorimetric recognition of pesticide dimethoate. Journal of Nanoparticle Research, 2016. 18(8): p. 233.